*Key Engineering Materials*
*ISSN: 1662-9795, Vol. 984, pp 1-7*
*doi:10.4028/p-CBuwR2*

*Submitted: 2023-09-30*
*Accepted: 2024-04-08*
*Online: 2024-08-22*

# Spin-Orbit Coupling of Color Centers for Quantum Applications

Mirjam Neubauer[a], Maximilian Schober[b], Witold Dobersberger[c], and Michel Bockstedte[d]

Institute for Theoretical Physics, Johannes Kepler University Linz, Altenbergerstr. 69, A-4040 Linz, Austria

[a]Mirjam.Neubauer@jku.at, [b]Maximilian.Schober@jku.at, [c]Witold.Dobersberger@gmx.at, [d]Michel.Bockstedte@jku.at

**Keywords:** Silicon Vacancy, Di-Vacancy, Qubit, Spin Relaxation Dynamics, *Ab Initio* Theory

**Abstract.** Color centers in 4H-SiC and diamond are candidates for single photon sources and qubits for the implementation of quantum applications. The CI-cRPA method is able to correctly reproduce the structure of the underlying highly correlated wave functions for low and high spin multiplets. Aiming for a more complete understanding of spin-orbit mediated intersystem crossing between such states, we have extended CI-cRPA by a first order treatment of the spin-orbit interactions. We present preliminary results for intercrossing matrix elements and contributions of spin-orbit coupling to the zero field splitting of the silicon vacancy and di-vacancy in 4H-SiC, as well as the NV center in diamond using this approach.

## Introduction

Silicon Carbide (4H-SiC) hosts vacancy-related color centers relevant for quantum application, such as the silicon vacancy ($V_{Si}$), di-vacancy ($V_C V_{Si}$), nitrogen-vacancy complex ($N_C V_{Si}$) and the carbon vacancy-antisite complex ($C_{Si} V_C$). The silicon vacancy gives rise to the V1, V1′ and V2 photoluminescence lines, and as a spin 3/2 system is distinct from the prototypical NV center in diamond ($S = 1$) or the isoelectronic $V_C V_{Si}$ and $N_C V_{Si}$. Naturally, the center has been the subject of intense experimental and theoretical effort to explore its potential as quantum bit. Optical manipulation of the spin includes the excitation of the fundamental quartet, and spin-selective non-radiative relaxation via intermediate doublet states facilitated by spin-orbit coupling [1, 2]. This together with the zero-field splittings of the ground and excited states enables a variety of spin-photon protocols towards the implementation of future quantum applications [3]. For optimal engineering of such interfaces, it is crucial to understand the spin-selective interactions for $V_{Si}$ and other color centers in general. The key question is, which of the intermediate states dominantly contribute to the spin-relaxation path.
Recent experiments [2] on silicon vacancies obtained the spin-dependent lifetimes and intercrossing rates of $V_{Si}$. The effective dynamics was described by only two intermediate states out of five of the theoretically predicted ones [4, 5]. Without a quantitative theoretical understanding of the spin-orbit coupling of this color center, the physics leading to these experimental results, however, cannot be satisfactorily unraveled.

## Theoretical Approach

Theoretical efforts aimed at the treatment of the spin-orbit coupling in potential quantum bits in 4H-SiC and diamond so far have been based on fundamental but parameter-dependent group theoretical analysis [4, 7] and density functional theory (DFT) [8]. Despite recent successes in predicting the zero-field splitting and the fine structure of the fundamental multiplet states, such approaches are not able to reproduce low-spin states pivotal for spin-orbit mediated spin dynamics. To overcome these limits, we have extended the *ab initio* framework of embedded configuration interaction (CI-CRPA) [9] by a first order treatment of spin-orbit coupling [10].
We first obtain ground state structures of the negatively charged silicon vacancy $V_{Si}^-$, the divacancy $V_C V_{Si}$ and the NV-center in diamond using spin-polarised DFT and the HSE06 hybrid exchange-correlation functional as implemented in VASP [11]. To mitigate finite size effects, we use supercells

containing up to 576 and 512 atoms for 4H-SiC and diamond respectively, which are sampled at the $\Gamma$ point. Spin unrestricted DFT calculations often suffer from spin contamination, leading to electronic states that are no longer eigenfunctions of the total spin operator. To circumvent this drawback, we therefore ground our CI calculations on a final electronic minimization in the relaxed supercells using non-polarised hybrid DFT. The CI basis is constructed from the resulting Kohn-Sham states, and encompasses valence and conduction band state close to the band edges, as well as, all defect resonances within the band gap [9, 5].
Slater determinants $\Phi_n$ formulated from this basis are constructed from a reference determinant by allowing all possible spin-flip excitations (full CI) within a set energy window, and restriction to single excitations outside the full-CI space.
The embedded hamiltonian of the defect is constructed on this basis and the effective Coulomb interaction $V_{\text{eff}}$ :

$$\hat{H} = \sum_{ij}(\epsilon_i\delta_{ij} - h_{ij}^{DC})\hat{a}_i^\dagger\hat{a}_j + \sum\langle ij|V_{\text{eff}}|nm\rangle\,\hat{a}_i^\dagger\hat{a}_j^\dagger\hat{a}_m\hat{a}_n, \tag{1}$$

where $h_{ij}^{DC}$ double counting correction (cf. [9]) and $V_{\text{eff}} = \epsilon_{\text{CRPA}}^{-1}\,V_{\text{Coulomb}}$ interaction within the constrained random phase approximation.The efficacy of this approach has been demonstrated in previous works [9]. Diagonalization of the associated Schrödinger matrix equation yields a set of eigenstates $\Psi_i$ of both the Hamiltonian and Spin-operator, composed of superpositions of the previously generated basis functions, of which each contributes by a complex coefficient $c_{in}$.
Subsequently, we turn on spin-orbit coupling for these pre-converged CI systems. The spin-orbit interaction between two CI states is written in terms of single particle matrix elements

$$H_{ij}^{\text{SOC}} = \langle\Psi_i|H^{\text{SOC}}|\Psi_j\rangle = \sum_{\Phi_m\in\Psi_i}\sum_{\Phi_n\in\Psi_j} c_{im}^* c_{jn}\langle\Phi_m|H^{\text{SOC}}|\Phi_n\rangle, \tag{2}$$

where $H^{\text{SOC}}$ is the Breit-Pauli single particle spin-orbit hamiltonian [10]. If states $i$ and $j$ belong to different spin manifolds (*e.g.* quartets and doublets in $V_{\text{Si}}^-$), finite values $H_{ij}^{\text{SOC}}$ indicate intersystem transitions between them are possible. In contrast, contributions of SOC to the zero-field splitting are assessed by diagonalizing a subset of (2), in which the indices $i$, $j$ are restricted to a group of CI-eigenstates that would be degenerate in the absence of SOC.
The contributions of different determinants in (2) follow the Slater Condon rules [12], and therefore require evaluation of matrix elements $\langle\phi_a|H^{\text{SOC}}|\phi_b\rangle$ between Kohn-Sham states $\phi_a$ and $\phi_b$ occupied within the determinants $\Phi_n$ and $\Phi_m$. For their calculation, we employ an in-house version of VASP in which the original PAW based implementation of Spin-Orbit coupling [13, 6] is modified to permit calculations of matrix elements

$$\langle\phi_a|H^{\text{SOC}}|\phi_b\rangle = \sum_I\sum_{\ell k}\langle\phi_{Ik}^{\text{AE}}|H^{\text{SOC}}|\phi_{I\ell}^{\text{AE}}\rangle\langle\phi_a^{\text{PS}}|p_{Ik}^{\text{PS}}\rangle\langle p_{I\ell}^{\text{PS}}|\phi_b^{\text{PS}}\rangle \tag{3}$$

using non-spin polarised (partial) wave functions and projectors with associated quantum numbers $k, \ell$ centered on the ions $I$.

**Correlated Spin States of the Silicon Vacancy and their Fine Structure**

We apply our approach to the prototypical negatively charged Silicon Vacancy $V_{\text{Si}}^-$ system in 4H-SiC. The electronic structure of the defect essentially arises from the interaction of the four carbon dangling bonds in the low symmetric crystal field of inequivalent cubic or hexagonal sites in 4H-SiC. The three half occupied single particle defect states $v$, $e_x$, $e_y$ and doubly occupied defect resonance $u$ form the $^4A_2$ groundstate quartet and $^4A_2'$, $^4E$ excited quartets, as well as intermediary doublets, as shown in Fig. 1. All these levels are strongly localized on the carbon atoms neighboring the vacancy. As such, they are expected to converge relatively quickly for increasing simulation cell sizes. In order to benchmark the influence of finite size effects on SOC, we have conducted non-collinear DFT calculations of multiple

defect supercells with varying sizes and shapes, containing between 199 and 2047 atoms employing the PBE exchange-correlation functional. Using the SOC energy contribution of the four defect states as a parameter, we find supercells containing $576$ atoms to be sufficiently converged while warranting effective usage of computational resources.

In Fig. 1 we show the defect level structure of the silicon vacancy on hexagonal (cubic) lattice sites obtained using regular CI-CRPA: alongside the $^4A_2$ ground state we find an excited $^4A_2'$ quartet at 1.501 eV (1.401 eV) and a $^4E$ quartet at 1.573 eV (1.519 eV). The corresponding zero phonon lines (ZPL) are found at 1.35 eV (1.25 eV) and 1.39 eV (1.32 eV) for the hexagonal (cubic) site. Due to the orbital degeneracy of the $^4E$ quartet and strong electron-phonon coupling in a dynamic Jahn-Teller effect, vibronic states arise from $^4A_2'$ and $^4E$ that explain the photo luminescence lines of $V_{Si}^-$ at the hexagonal (V1, V1' lines) and the cubic (V2 line) lattice sites [8]. The experimental values for V1, V1' and V2 are 1.439 eV, 1.445 eV and 1.35 eV [14].

Within the spin doublet manifold, three groups of multiplet states ($^2E$, $^2A_2$ and $^2E'$, as well as $^2E''$, $^2A_2'$) are identified at intermediary energies between the ground and excited quartets. While the existence and highly correlated nature of these fundamental symmetry-adapted states has been predicted recently [4, 5, 15], their representation within *ab initio* frameworks has traditionally been difficult. In Table 1 we decompose the CI doublets of $E$-character into the initial doublets predicted by group theory [15].

Table 1: Projections of CI $^2E$ doublets (see Fig. 1) on symmetry adapted doublet wavefunctions ($d1-d8$) based on group theory [15]. States such as $\Psi^2_{d1}$ not explicitly listed here contribute symmetrically, *e.g.* $\Psi^4_{^2E} \propto \mathrm{i}0.307|\Psi^2_{d1}\rangle$.

| $^2E$ | $\Psi^1_{d1}$ | $\Psi^3_{d1}$ | $\Psi^1_{d3}$ | $\Psi^3_{d3}$ | $\Psi^1_{d5}$ | $\Psi^3_{d5}$ | $\Psi^1_{d6}$ | $\Psi^3_{d6}$ | $\Psi^1_{d8}$ | $\Psi^3_{d8}$ |
|---|---|---|---|---|---|---|---|---|---|---|
| $\Psi^1_{^2E}$ | 0.307i | -0.217i | -0.387i | 0.547i | -0.262 | -0.185 | -0.191i | | | |
| $\Psi^2_{^2E}$ | 0.309 | 0.218 | 0.386 | 0.545 | 0.264i | -0.186i | -0.191 | | | |
| $\Psi^3_{^2E}$ | | 0.217 | 0.387 | | | -0.185i | | -0.191i | | |
| $\Psi^4_{^2E}$ | | -0.218i | 0.386i | | | 0.186i | | 0.191 | | |
| $\Psi^1_{^2E'}$ | -0.423i | 0.299i | -0.250i | 0.353i | 0.229 | 0.162 | -0.003i | | 0.175i | -0.248i |
| $\Psi^2_{^2E'}$ | -0.422 | -0.298 | 0.251 | 0.355 | -0.229i | 0.162i | -0.003 | | -0.175 | -0.247 |
| $\Psi^3_{^2E'}$ | | -0.262 | 0.218 | | | 0.221i | | -0.001 | -0.153 | |
| $\Psi^4_{^2E'}$ | | 0.147 | -0.123 | | | 0.062i | | -0.002 | 0.086 | |
| $\Psi^1_{^2E''}$ | -0.373 | -0.264 | | | 0.058 | 0.041 | | | -0.075 | -0.106 |
| $\Psi^2_{^2E''}$ | 0.373i | -0.264i | | | 0.535 | 0.379 | 0.002i | | -0.074i | 0.105i |
| $\Psi^3_{^2E''}$ | | -0.046 | | | | -0.441i | | -0.002 | 0.074i | |
| $\Psi^4_{^2E''}$ | | 0.261 | | | | 0.309i | | 0.002i | 0.074 | |

Using the listed coefficients, all of the CI states can therefore be represented by the fundamental symmetry adapted states. Our corresponding analysis of the excited quartet geometries indicates a strong electron-phonon coupling between these doublet states with small energy separation as suggested earlier [4, 15, 2] and already described for the di-vacancy and NV-center in diamond [9].

The introduction of spin-orbit interaction leads to a fine structure of the degenerate quartets and doublets, as well as, a dynamic coupling among the quartet and doublet spin manifolds. As a first step, we calculate the SOC induced fine structure of the three considered quartet states. Consistent with group theory, no splitting is obtained for the $^4A_2$ and $^4A_2'$ states, while the $^4E$ states split into 4 distinct

components separated equally by an energy $\Delta = 106\ \mu$eV and $\Delta = 148\ \mu$eV for the hexagonal and cubic site respectively. Notably, these results are in good agreement with extrapolated values 96 $\mu$eV and 136 $\mu$eV for infinite cell sizes based on ${}^4E$ splittings obtained within DFT [8]. Note that motional effects due to the dynamic Jahn-Teller coupling in the ${}^4E$ states may reduce these values (Ham effect).

In Tab. 2 we provide the intercrossing matrix elements between the the quartet ground and first excited quartet state and the 5 spin doublet states for the hexagonal silicon vacancy. Here we focus on the coupling of the ${}^4A_2$ and ${}^4A_2'$ quartets with the doublets, as in the experiments, the optical cycle is usually driven via the corresponding V1 and V2 lines. Taking the composition of the doublet states into account we find consistency with earlier group theory analysis [4] regarding transition matrix elements. In particular, the coupling of both quartets to the ${}^2A_2$ states is forbidden. We furthermore note that the transition matrix elements from the quartet sublevels with $m_s = \pm\frac{3}{2}$ to the doublets with $E$ symmetry are approximately twice as large compared to the coupling to the sublevels with $m_s = \pm\frac{1}{2}$. Although this is also true for $V^-_{Si,c}$ different magnitudes occur. This indicates the existence of a spin contrast in the fluorescence. However this is manifested requires further analysis. Given the vibronic nature of the ${}^4E$ quartet, the treatment of its SOC requires a more involved analysis which is beyond the scope of this work.

Recent analysis of experiments on the spin-relaxation cycle have demonstrated a successful description via two effective metastable states [2, 1]. Our theoretical approach instead finds three groups of doublets. As mentioned above, we have indications for a strong electron-phonon coupling between these states, together with the calculated SOC parameters that should allow for an effective description of the spin-relaxation dynamics by a reduced number of metastable states.

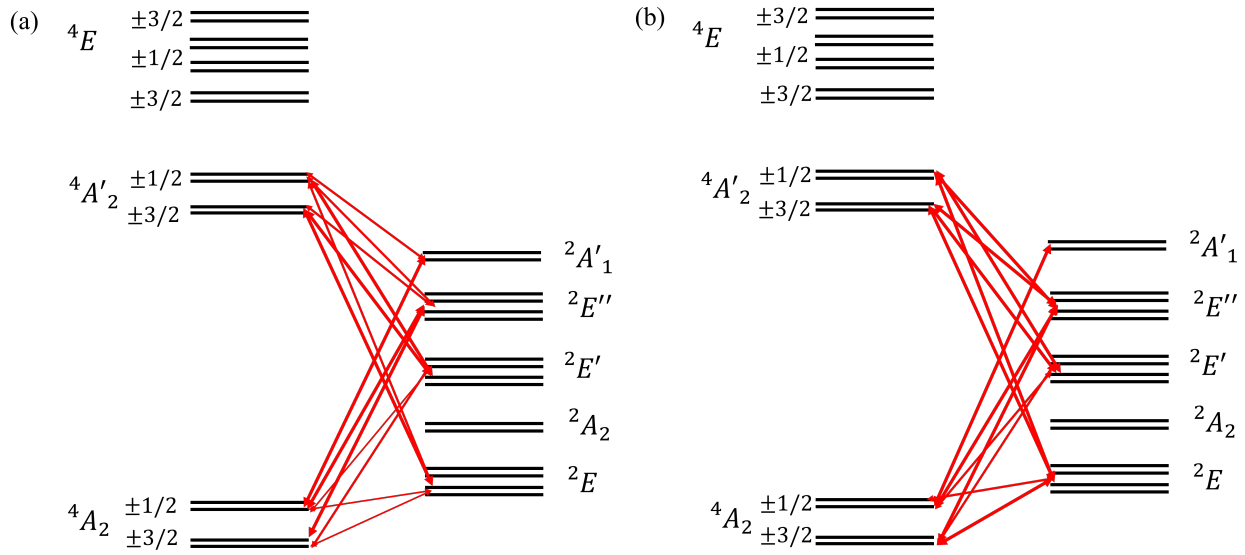


Fig. 1: Defect level structure and spin-orbit coupling between doublets (right) and quartets (left) of the negatively charged Silicon vacancy at (a) hexagonal and (b) cubic lattice sites. The separation between the magnetic sub-levels is introduced for readability only. Numeric values for the matrix elements between the ${}^4A_2$ quartets and the intermediate doublets of $V^-_{Si,h}$ are specified in Table 2.

### Fine Structure of NV-Center in Diamond and the Di-Vacancy in 4H-SiC

Besides $V_{Si}$, we also address the hexagonal axial di-vancancy in 4H SiC as well as the $NV^-$-center in diamond. Application of CI-CRPA on these centers has already been successfully demonstrated to reproduce their electronic structure and zero phonon lines [9]. Therefore, we only note here, that for all systems the states typically accessed in experimental settings consists of ${}^3A_2$ ground and ${}^3E$ excited states in the spin triplet domain, while two singlets (${}^1E$, ${}^1A_1$) are found at intermediary energies

Table 2: Spin-Orbit matrix elements (absolute values) between ground and first excited quartet and intermediary doublet states for $V^-_{Si,h}$ in $\mu$eV. Elements with relatively small magnitudes $< \varepsilon = 0.1$ $\mu$eV are unlikely to contribute significantly, and hence are not explicitly provided.

| $V^-_{Si,h}$ | $\Psi^1_{^4A_2}$ | $\Psi^2_{^4A_2}$ | $\Psi^3_{^4A_2}$ | $\Psi^4_{^4A_2}$ | $\Psi^1_{^4A'_2}$ | $\Psi^2_{^4A'_2}$ | $\Psi^3_{^4A'_2}$ | $\Psi^4_{^4A'_2}$ |
|---|---|---|---|---|---|---|---|---|
| $\Psi^1_{^2E}$ | 9.47 | $< \varepsilon$ | 5.47 | 0 | 19.37 | $< \varepsilon$ | 11.18 | 0 |
| $\Psi^2_{^2E}$ | 9.54 | 1.52 | 5.51 | 0 | 18.44 | 1.30 | 10.65 | 0 |
| $\Psi^3_{^2E}$ | 0 | 5.51 | 1.50 | 9.54 | 0 | 10.67 | 1.28 | 18.48 |
| $\Psi^4_{^2E}$ | 0 | 5.47 | 0.28 | 9.48 | 0 | 11.16 | 0.24 | 19.34 |
| $\Psi^1_{^2A_2}$ | $< \varepsilon$ | $< \varepsilon$ | $< \varepsilon$ | 0 | 0.18 | $< \varepsilon$ | 0.11 | 0 |
| $\Psi^2_{^2A_2}$ | 0 | $< \varepsilon$ | $< \varepsilon$ | $< \varepsilon$ | 0 | 0.11 | $< \varepsilon$ | 0.18 |
| $\Psi^1_{^2E'}$ | 57.60 | 8.82 | 33.25 | 0 | 15.90 | 3.41 | 9.18 | 0 |
| $\Psi^2_{^2E'}$ | 59.01 | 0.57 | 34.07 | 0 | 18.61 | 0.22 | 10.75 | 0 |
| $\Psi^3_{^2E'}$ | 0 | 33.25 | 8.84 | 57.60 | 0 | 9.17 | 3.41 | 15.89 |
| $\Psi^4_{^2E'}$ | 0 | 34.07 | $< \varepsilon$ | 59.01 | 0 | 10.75 | $< \varepsilon$ | 18.62 |
| $\Psi^1_{^2E''}$ | 280.28 | 4.60 | 161.82 | 0 | 38.64 | 0.57 | 22.31 | 0 |
| $\Psi^2_{^2E''}$ | 278.57 | 0.21 | 160.83 | 0 | 34.18 | $< \varepsilon$ | 19.73 | 0 |
| $\Psi^3_{^2E''}$ | 0 | 161.82 | 4.18 | 280.28 | 0 | 22.31 | 0.51 | 38.64 |
| $\Psi^4_{^2E''}$ | 0 | 160.84 | 0.14 | 278.57 | 0 | 19.74 | $< \varepsilon$ | 34.18 |
| $\Psi^1_{^2A'_1}$ | 2.27 | 252.79 | 1.31 | 0 | $< \varepsilon$ | 36.54 | $< \varepsilon$ | 0 |
| $\Psi^2_{^2A'_1}$ | 0 | 1.04 | 252.79 | 1.81 | 0 | $< \varepsilon$ | 36.54 | $< \varepsilon$ |

between the triplets. In Fig. 2 we summarize electronic structures and the SOC transition matrix elements between triplets and singlets. The absolute values of the matrix elements are provided in Table 3 for both defects. Due to the admixture of the $^1E'$ singlet to the $^1E$ singlet [9] and the finite spin-orbit coupling between the $^1E'$ singlet and the $m_s = \pm 1$ levels of the groundstate [16] a finite spin orbit coupling between the $\pm 1$ state of the $^3A_2$ triplet is given. This is not contained in [7].

Regarding the fine structure, consistent with group theory no SOC contribution to the fine structure is found for the $^3A_2$ state. For the excited $^3E$ triplets of the NV center we obtain a threefold splitting of $0.17$ meV. This corresponds to a coupling constant $\lambda_{\|} = 20.6$ GHz. This is somewhat larger than the value of $15.8$ GHz obtained via in hybrid-DFT [17] extrapolated to infinite supercell sizes. The discrepancy to the experimental results (5.3 GHz [18]) arises from motional quenching by the dynamic Jahn-Teller effect.

## Summary

In summary, we have analyzed the spin orbit interaction of the negatively charged silicon vacancy, the di-vacancy in 4H SiC, and the NV-center in diamond. We focused on the contributions to the fine structure as well as the coupling between high and intermediate low spin multiplets. The latter is a key for understanding the non-radiating spin-relaxation dynamics. The investigation was conducted in the many-electron embedding CI-cRPA approach that is able to describe the ground and excited multiplet

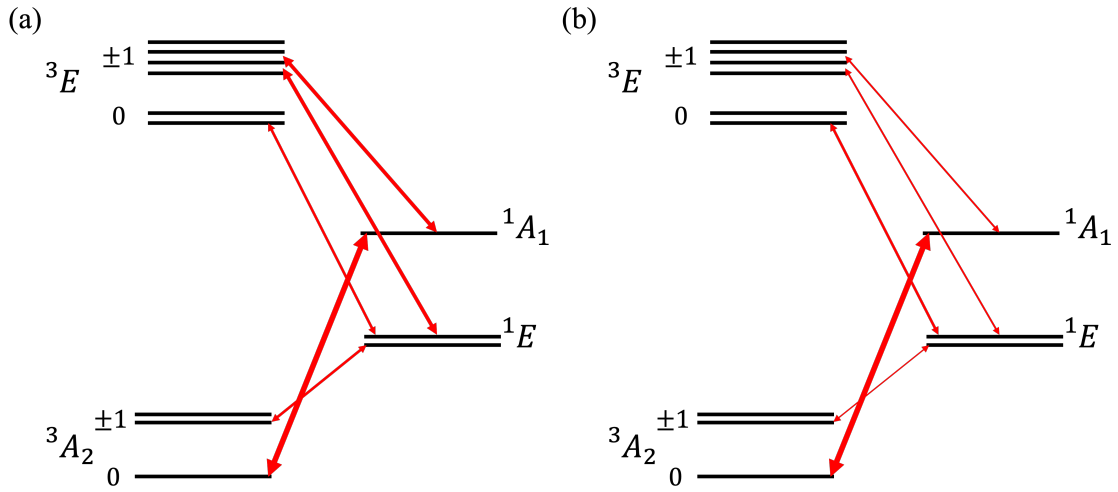


Fig. 2: Eletronic structure and intersystem coupling between triplets and singlets of (a) the NV center in diamond and (b) the axial hexagonal di-vacancy $V_C V_{Si}$ in 4H-SiC. The separation between the magnetic sub-levels is introduced for readability only. Numeric values for the matrix elements are specified in Table 3.

Table 3: Spin-Orbit matrix elements (absolute values) of the $^3A_2$ and $^3E$ triplet with intermediary singlet states in axial hexagonal $V_C V_{Si}$ and the NV-center in diamond, given in units of $\mu$eV. Elements with tiny magnitudes $< \varepsilon = 0.1$ $\mu$eV are not given explicitly.

| | | $\Psi^1_{^3A_2}$ | $\Psi^2_{^3A_2}$ | $\Psi^3_{^3A_2}$ | $\Psi^1_{^3E}$ | $\Psi^2_{^3E}$ | $\Psi^3_{^3E}$ | $\Psi^4_{^3E}$ | $\Psi^5_{^3E}$ | $\Psi^6_{^3E}$ |
|---|---|---|---|---|---|---|---|---|---|---|
| NV | $\Psi^1_{^1E}$ | 53.70 | $< \varepsilon$ | 53.70 | 201.20 | 201.20 | 3.71 | 48.06 | 201.20 | 201.20 |
| | $\Psi^2_{^1E}$ | 53.70 | $< \varepsilon$ | 53.70 | 201.20 | 201.20 | 48.06 | 3.71 | 201.20 | 201.20 |
| | $\Psi^1_{^1A_1}$ | $< \varepsilon$ | 372.50 | $< \varepsilon$ | 173.50 | 173.50 | $< \varepsilon$ | $< \varepsilon$ | 173.50 | 173.50 |
| $V_C V_{Si,hh}$ | $\Psi^1_{^1E}$ | 19.76 | 0.23 | 19.76 | 41.32 | 41.65 | 2.45 | 53.36 | 41.32 | 41.65 |
| | $\Psi^2_{^1E}$ | 19.84 | $< \varepsilon$ | 19.84 | 41.86 | 41.65 | 53.21 | 2.45 | 41.86 | 41.65 |
| | $\Psi^1_{^1A_1}$ | $< \varepsilon$ | 366.66 | $< \varepsilon$ | 2.32 | 1.76 | $< \varepsilon$ | $< \varepsilon$ | 2.32 | 1.76 |

states consistently. Our analysis of the silicon vacancy goes beyond previous group theory analysis and DFT approaches in unveiling the composition of the intermediate highly correlated doublet states and their coupling to the fundamental quartet states. This revises earlier spin orbit coupling path schemes due to extensive hybridization of the metastable doublet states. Related couplings for the NV center in diamond and the iso-electronic di-vacancy in 4H SiC appear between the $^1E$ singlet and the ground state earlier considered without invoking electron-phonon coupling. Our approach together with an implementation to the electron-phonon coupling will give access to a fully-fledged treatment of the spin-relaxation cycle in such complex cases as the silicon vacancy.

**Acknowledgment**

The authors received financial support from the Austrian Science Fund (FWF, grant I5195) and German Research Foundation (DFG, QuCoLiMa, SFB/TRR 306, Project No. 429529648). The project profited from very generous computer time provided by the Erlangen National High Performance Computing Center (NHR@FAU) of the Friedrich-Alexander-Universität Erlangen-Nürnberg (FAU) and the Vienna Scientific Cluster (VSC).

**References**

[1] H. Kraus et al, Nat. Phys **10**, 157 (2014) .

[2] N. Morioka et al.Phys. Rev. Appl. **17** 054005 (2022) .

[3] R. Nagy et al., Nat. Commun. **10** 1954 (2019) .

[4] Ö. O. Soykal, P. Dev, and S. E. Economou, Phys. Rev. B **93** 081207(R) (2016) .

[5] M. Widmann et al., Nano Lett. **19** 7173-7180 (2019) .

[6] E. van Lenthe, E. J. Baerends, and J. G. Snijders, J. Chem. Phys. **99** 4597–4610 (1993) .

[7] J. R. Maze et al, New J. Phys. **13** 025025 (2011) .

[8] P. Udvarhelyi et al., Phys. Rev. Applied **13** 054017 (2020) .

[9] M. Bockstedte, et al., npj Quant Mater **3**, 31 (2018) .

[10] N. Bellonzi et al., J. Chem. Phys. **150** 014106 (2019) .

[11] G. Kresse and J. Furthmüller, Phys. Rev. B **54** 11169 (1996). G. Kresse and D. Joubert, Phys. Rev. B **59** 1758 (1999) .

[12] A. Szabo and N. S. Ostlund, (2012). Modern quantum chemistry: introduction to advanced electronic structure theory. Courier Corporation.

[13] S. Steiner, S. Khmelevskyi, M. Marsmann, and G. Kresse, Phys. Rev. B **93** 224425 (2016) .

[14] E. Janzén, Physica B **404**, 4354 (2009) .

[15] W. Dong, M. W. Doherty, and S. E. Economou, Phys. Rev. B **99**, 184102 (2019) .

[16] M.W. Doherty, N.B. Manson, P. Delaney, and L. C. L. Hollenberg, New Journal of Physics **13**, 025019 (2011) .

[17] G. Thiering and A. Gali, Phys. Rev. B **96**, 081115(R) (2017) .

[18] A. Batalov et al., Phys. Rev. Lett. **102**, 195506 (2009) .